Scale Invariance of a Spherical Unitary Fermi Gas

Lu Wang,[1,2] Xiangchuan Yan,[1] Jing Min,[1,2] Dali Sun,[1,*] Xin Xie,[1,2] Shi-Guo Peng,[1]
Mingsheng Zhan,[1] and Kaijun Jiang[1,†]

[1]*State Key Laboratory of Magnetic Resonance and Atomic and Molecular Physics,*
Innovation Academy for Precision Measurement Science and Technology,
Chinese Academy of Sciences, Wuhan 430071, China
[2]*University of Chinese Academy of Sciences, Beijing 100049, China*

A unitary Fermi gas in an isotropic harmonic trap is predicted to show scale and conformal symmetry that have important consequences in its thermodynamic and dynamical properties. By experimentally realizing a unitary Fermi gas in an isotropic harmonic trap, we demonstrate its universal expansion dynamics along each direction and at different temperatures. We show that as a consequence of SO(2,1) symmetry, the measured release energy is equal to that of the trapping energy. We further observe the breathing mode with an oscillation frequency twice the trapping frequency and a small damping rate, providing the evidence of SO(2,1) symmetry. In addition, away from resonance when scale invariance is broken, we determine the effective exponent γ that relates the chemical potential and average density along the BEC-BCS crossover, which qualitatively agrees with the mean field predictions. This Letter opens the possibility of studying nonequilibrium dynamics in a conformal invariant system in the future.

Strongly interacting Fermi gases are created by tuning the interaction strength between atoms of different spin states via Feshbach resonance [1,2]. The unitary Fermi gas, realized when the *s*-wave scattering length is tuned to infinity, is of special interest in various geometries including harmonic [3–7] and box traps [8–11]. It is not only strongly correlated but also an example of a scale-invariant quantum many-body system. One of the basic tools used to explore the properties of unitary Fermi gas is the expansion dynamics [12] and much insight has been obtained about the role of interactions [13–15].

The strongly interacting Fermi gas at finite temperature is described by a hydrodynamic theory [see Eq. (1)], where the transport behaviors are determined by viscosities [16–18]. At unitarity, the bulk viscosity ζ_B vanishes, and the friction force arise from shear viscosity η. For a unitary Fermi gas in an anisotropic trap studied previously, the conformal symmetry is broken and the shear viscosity plays a dominant role, which allowed its extraction from expansion dynamics [19–21]. On the other hand, for a spherical unitary Fermi gas, the transverse relative motion of the atomic cloud is absent ($\sigma_{ii} = 0$), and consequently the effect of the shear viscosity can be neglected. The system without viscosity contribution would have scale invariance of the mean square cloud radius $\langle x^2 \rangle \to \lambda^2 \langle x^2 \rangle$ under the transformation $x \to \lambda x$, being connected to a noninteracting gas. Contrary to the anisotropic system, the spherical unitary Fermi gas has a hidden SO(2,1) symmetry [22,23] with Hamiltonian and raising and lowering operators composing three parts of the SO(2,1) Lie algebra,

which predicts the exact relations between trapping potential energy and total energy and the breathing mode with an oscillation frequency twice the trapping frequency. However, the preparation and exploration of the universal properties of a spherical unitary Fermi gas are yet to be demonstrated experimentally.

In this Letter, we produce a spherical Fermi gas in an optical dipole trap (ODT) and explore scale invariant behaviors in strongly interacting regimes. By tuning the interaction strength to unitarity, the expansion of the system shows the scale invariance along each direction and at different temperatures, which is absent in an anisotropic system. We find that the trapping potential energy equals to the half of the total energy, verifying the virial theorem at unitarity. Furthermore, we observe the breathing mode with an oscillation frequency twice the trapping frequency and a small damping rate, providing the evidence of SO(2,1) symmetry [22]. In addition, we explore expansion dynamics away from unitarity when scale invariance is broken, and measure the effective exponent γ of $\mu(n) \propto n^\gamma$ where μ is the chemical potential and n is the average density. To the best of our knowledge, this is the first experiment on the 3D ultracold quantum gases with SO(2, 1) symmetry.

The expansion of strongly interacting Fermi gases is described by the hydrodynamic theory [14,19,23]

$$\frac{d^2}{dt^2}\frac{m\langle x_i^2 \rangle}{2} = \left\langle x_i \frac{\partial U}{\partial x_i}\right\rangle_0 + \frac{1}{N}\int d^3r[\Delta p - \Delta p_0]$$
$$- \frac{1}{N}\int d^3r(\eta\sigma_{ii} + \zeta_B\sigma'), \qquad (1)$$

where $\langle x_i^2 \rangle$ represents the mean square cloud radius along the ith axis ($i = x, y, z$), U is the trapping potential, t is the expansion time, the subscript $(_0)$ denotes the initial condition in the trap at $t = 0$, and $\Delta p = p - (2/3)\varepsilon$ is the scale-invariance breaking pressure, where ε is the energy density [27]. The last term on the right describes the friction forces arising from shear viscosity η and bulk viscosity ζ_B. Here, $\sigma_{ii} = 2\dot{b}_i/b_i - (2/3)\sum_j \dot{b}_j/b_j$ represents the transverse relative motion and $\sigma' = \sum_i \dot{b}_i/b_i$ for the dilation process, where b_i denotes the expansion scale factor. In the unitary regime, both Δp and ζ_B vanish [19,28–30]. The value of σ_{ii} depends on the geometry or symmetry of the atomic cloud. Only for a spherical gas, the relative motion is absent with $\sigma_{ii} = 0$, and in this case, we obtain the expansion behavior

$$\langle x_i^2 \rangle = \langle x_i^2 \rangle_0 + \frac{t^2}{m}\left\langle x_i \frac{\partial U}{\partial x_i} \right\rangle_0. \tag{2}$$

Equation (2) shows the ballistic expansion analogous to a noninteracting ideal gas, and the interaction is included in the *in situ* atomic cloud size $\langle x_i^2 \rangle_0$.

The scale-invariant expansion along each direction can be tested by determining the value

$$\tau_i^2(t) = \frac{\langle x_i^2 \rangle_t - \langle x_i^2 \rangle_0}{\langle x_i^2 \rangle_0 \omega^2}, \tag{3}$$

where $\omega_x = \omega_y = \omega_z = \omega$ is the trapping frequency. According to Eq. (2), $\tau^2(t) = t^2$. The ideas of using ballistic expansion and $\tau^2(t)$ as measure of scale invariance were suggested and demonstrated experimentally in an anisotropic Fermi gas [14], where only sum of mean square radii along three axes shows the scale invariance.

We prepare a spherical Fermi gas based on our previous works [31,32]. We initially prepare a ^{6}Li atomic degenerate Fermi gas with two spin states $|F = 1/2, m_F = \pm 1/2\rangle$ in an elongated ODT and at the Feshbach-resonance magnetic field of 834 G. The experimental setup of the isotropic trap is schematically displayed in Fig. 1(a), where some special techniques are applied. First, a magnetic field with a gradient $B_z' = 1.05$ G/cm is applied along z axis to simultaneously compensate the gravity force of the two spin states. This is valid for ^{6}Li atoms because the hyperfine interaction is much smaller than the Zeeman shift at the applied magnetic field. Second, two elliptic optical beams with a cross-sectional aspect ratio of $\sqrt{2}$, propagating perpendicularly in the horizontal plane, form the isotropic trap. Under these conditions, the trapping frequency can be varied by adjusting the optical power (see Supplemental Material [23] for details). We transfer the unitary Fermi gas to the isotropic trap with an efficiency of more than 90%. After performing the evaporative cooling in the isotropic trap, we slowly increase the optical power to 3.8 W in about 75 ms.
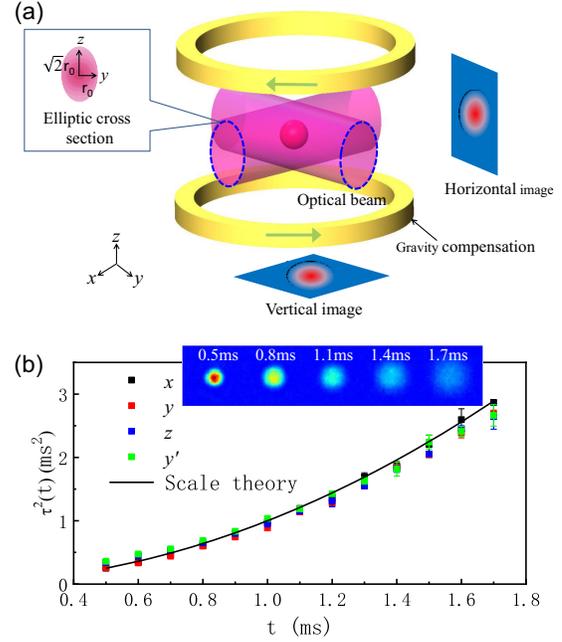
FIG. 1. Production of a spherical Fermi gas and scale-invariant expansion along each direction. (a) Schematics of the experimental setup. Two elliptic optical beams, propagating along x and y axes, respectively, form the isotropic trap. The ratio of the beam width along z direction to that in the horizontal plane is $\sqrt{2}$. A pair of anti-Helmholtz coils produce a gradient magnetic field along vertical direction to compensate the gravity. Another pair of Helmholtz coils (not shown) produces a homogeneous magnetic field along vertical direction to tune the interactions. (b) Values of $\tau_i^2(t)$ versus the expansion time t along different directions ($i = x, y, z, y'$). The inset shows typical atomic images taken in the vertical direction, where the expansion time is 0.5, 0.8, 1.1, 1.4, and 1.7 ms. y' direction is between x and y axes. The error bar is the standard deviation of several measurements. The black solid curve represents the scale theory $\tau^2(t) = t^2$. $T/T_F = 0.36(3)$, where T_F is the Fermi temperature of the noninteracting Fermi gas.

The temperature is adjusted by controlling the optical power of the evaporative cooling. The atom number is $N = 2.9(3) \times 10^4$ and the spin polarization is less than 6%. The trapping frequencies are $(\omega_x, \omega_y, \omega_z) = 2\pi \times [1234(6), 1165(11), 1204(3)]$ Hz, which are nearly the same along three axes [23].

We switch off the isotropic ODT and measure the cloud width versus the expansion time t at the magnetic field $B = 834$ G. Two laser beams with a frequency difference of 76 MHz, propagating along vertical and horizontal directions, respectively, are applied to detect two spin states. Typical atomic images during the expansion are shown in the inset of Fig. 1(b), indicating an isotropic expansion in direct contradiction to an elongated Fermi gas [2]. We use a fringe-removal algorithm [23,33] to reduce the imaging noise. The cloud radius $\langle x_i^2 \rangle_t$ is obtained by fitting a Gaussian distribution to the atomic density profile.
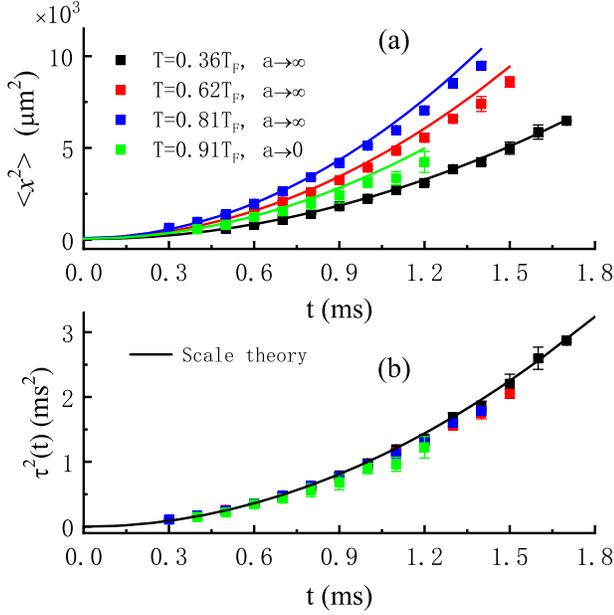
FIG. 2. Scale-invariant expansion at different temperatures. (a) Atomic cloud size $\langle x^2(t)\rangle$ versus the expansion time t in the unitary regime ($a \to \infty$). $T/T_F = 0.36(3)$ (black), 0.62(2) (red), and 0.81(2) (blue), respectively. For comparison, the noninteracting Fermi gas ($a \to 0$) is also shown with $T/T_F = 0.91(3)$ (green). The solid curves represent the calculations of Eq. (2). The error bar is the standard deviation of several measurements. (b) Values of $\tau^2(t)$ versus the expansion time t at different temperatures. The solid black curve denotes the scale theory $\tau^2(t) = t^2$.

In the unitary regime, the temperature is determined by analyzing the atomic density distribution, and the cloud radius in the trap $\langle x_i^2 \rangle_0$ can be theoretically calculated [3,23,31]. Values of $\tau^2(t)$ are calculated according to Eq. (3). As shown in Fig. 1(b), the expansion behaviors along different directions all obey the scale theory $\tau^2(t) = t^2$, which indicates the absence of the effect of viscosity. This scale-invariant expansion along each direction is unique for a spherical Fermi gas.

In Fig. 2, we measure the atomic expansion at different temperatures. Only expansion along the x axis is displayed for simplicity. Because of the finite-temperature effect, the atomic cloud size $\langle x^2(t)\rangle$ shows an obvious difference, as shown in Fig. 2(a). System at a higher temperature has a larger *in situ* cloud radius $\langle x_i^2 \rangle_0$, leading to a faster expansion, which agrees well with the theoretical prediction of Eq. (2). While values of $\tau^2(t)$ at different temperatures are consistent, all obeying the scale theory $\tau^2(t) = t^2$ [see Fig. 2(b)]. For comparison, the expansion behavior of a noninteracting Fermi gas ($a \to 0$, where a is the s-wave scattering length) is also shown. The Fermi gas in the unitary regime ($a \to \infty$) has the same scaled expansion behavior with that of the noninteracting Fermi gas.
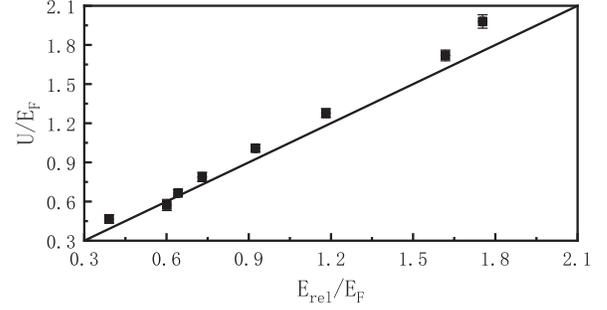
FIG. 3. Verifying the virial theorem for a unitary Fermi gas. The trapping potential U shows a linear dependence on the release energy E_{rel}. The error bar of the trapping potential comes from the uncertainty of the trapping frequency. The error bar of the release energy from the standard deviation of several measurements is smaller than the mask size. Both energies are normalized by the Fermi energy $E_F = (3N)^{1/3}\hbar\omega$, where N is the atom number and ω is the trapping frequency. The solid line represents the relation $U = E_{rel}$.

As predicted by SO(2,1) symmetry, the total energy should be twice the trapping potential energy [22]. This energy relation, which is called the virial theorem, also could be derived based on the equation of state and verified by measuring the trapping potential energy [13]. Here, we verify the virial theorem using the expansion method. The total energy of the trapped gas is the sum of trapping potential energy U, kinetic energy E_{kin}, and interaction energy E_{int}, $E_{tot} = U + E_{kin} + E_{int}$. After switching off the trapping potential ($U = 0$), the release energy $E_{rel} = E_{kin} + E_{int}$ remains constant during the expansion [34–36] and will be completely converted to the kinetic energy in the long-time expansion. So we only need to demonstrate the relation $U = E_{rel}$. By fitting the slope of atomic cloud radius respect to the expansion time, we obtain the release energy $E_{rel} = (3/2)mv_x^2$, where v_x is the expansion velocity along x axis. We can also determine the trapping potential energy $U = (3/2)m\omega^2\langle x^2 \rangle_0$, which varies with atomic temperature. The experimental results are shown in Fig. 3, where the atomic temperature changes across the Fermi degeneracy. The virial theorem is valid over a wide range of energies.

Next we will study the breathing mode, demonstrating SO(2,1) symmetry of the system at unitarity. To excite the breathing mode, we sinusoidally modulate the optical field at twice the trapping frequency for four periods, making the atomic cloud sizes oscillate in phase along three axes. After different holding times t in the trap, the atomic cloud is imaged with a time of flight of 1 ms. The breathing mode oscillation is defined as

$$A_B = \frac{\sum_i \langle x_i^2 \rangle(t)}{\langle \sum_i \langle x_i^2 \rangle(t)\rangle} - 1, \qquad (i = x, y, z), \qquad (4)$$
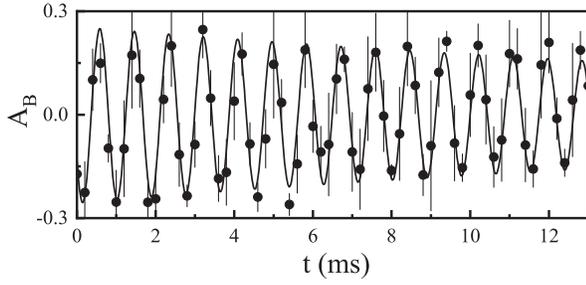
FIG. 4. Breathing oscillation as a function of the holding time t in the trap. Experimental data are fitted with a damped sinusoidal function (solid curve). The oscillation frequency is $\omega_B = 2\pi \times 1142(2)$ Hz $\approx 2\omega_0$ and the damping rate is $\Gamma_B = 38(8)$ s^{-1}. Error bar is the standard deviation of several measurements. Here, the temperature is $T/T_F = 0.29(1)$ and the mean trapping frequency is $\omega_0 = 2\pi \times 583$ Hz.

where $\langle x_i^2 \rangle(t)$ is the mean square cloud radius and $\langle \sum_i \langle x_i^2 \rangle(t) \rangle$ is the average value of all data. As shown in Fig. 4, the oscillation is fitted with a damped sinusoidal function $A_B = \delta A_B \sin(\omega_B t + \phi) \exp(-\Gamma_B t)$. Here, the mean trapping frequency along three axes is $\omega_0 = 2\pi \times 583$ Hz. The oscillation frequency is $\omega_B = 2\pi \times 1142(2)$ Hz $\approx 2\omega_0$ and the damping rate is $\Gamma_B = 38(8)$ s^{-1}. The normalized damping rate to the oscillation frequency is very small, i.e., $\Gamma_B/\omega_B \approx 0.005(1)$. Observation of the breathing mode with an oscillation frequency twice the trapping frequency and a small damping rate provides a direct evidence of SO(2,1) symmetry [22]. The SO(2,1) symmetry in a 2D quantum gas has also been demonstrated in a similar way [37–39].

For comparison, we measure the breathing mode away from the unitarity. On the BEC side ($1/k_Fa = 0.57$), the oscillation frequency is $\omega_B \approx 2.08\omega_0$ and the normalized damping rate is $\Gamma_B/\omega_B \approx 0.009(1)$. On the BCS side ($1/k_Fa = -0.84$), the oscillation frequency is $\omega_B \approx 1.94\omega_0$ and the normalized damping rate is $\Gamma_B/\omega_B \approx 0.006(1)$. Away from the unitarity, the ratio of the oscillation frequency to the trapping frequency is not equal to 2 and the damping rate increases more or less. The difference from the unitarity is large on the BEC side and small on the BCS side, which is similar to the measurements of the free expansion (see Fig. 5).

Away from the resonance with $\Delta p \neq 0$, the scale invariance will be broken. We assume a power-law dependence of the chemical potential, $\mu(n) = n^\gamma$, where n is the average atomic density and γ is the effective exponent [40–42]. By imposing that the total energy variation vanishes to first order, one gets the energy relation in the BEC-BCS crossover [41], $3\gamma E_{\mathrm{rel}} = 2U$. Considering that the bulk viscosity is negligibly small [14] and the effect of the shear viscosity in a spherical system is zero, we obtain the expansion scale factors [40]

$$\ddot{b}_i - (\omega^2/b_i)\Gamma^{-\gamma} = 0, \tag{5}$$
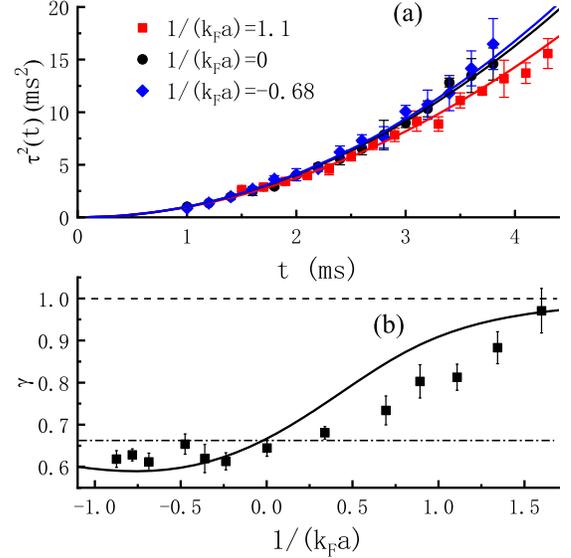
FIG. 5. Scale-invariance breaking in the BEC-BCS crossover. (a) Values of $\tau^2(t)$ versus the expansion time t at different interactions. The expansion behaviors are represented for BEC ($1/k_Fa = 1.1$, red squares), unitary ($1/k_Fa = 0$, black circles), and BCS ($1/k_Fa = -0.68$, blue diamonds) regions, respectively. The solid curves denote the calculations of Eq. (6) with experimentally obtained γ. In the unitary regime, $T/T_F = 0.21(2)$. (b) Values of γ in the BEC-BCS crossover. The solid curve depicts the mean field calculation at zero temperature as in Ref. [40]. The dashed line denotes $\gamma = 1$ valid deeply in the BEC regime, and the dot-dashed line denotes $\gamma = 2/3$ valid at unitarity and deeply in the BCS regime.

where $\Gamma = b_i^3$. Equation (5) is a decoupled equation for each direction, where b_i can be calculated if one knows the value of γ. In the unitary regime with $\gamma = 2/3$, Eq. (5) has an analytical solution the same as Eq. (2). In the BEC-BCS crossover, $\tau^2(t)$ can be calculated as

$$\tau^2(t) = \frac{b_i^2 - 1}{\omega^2}. \tag{6}$$

To measure γ at different interactions, we adiabatically ramp the magnetic field from 834 G to the desired value in 300 ms. As the power-law dependence of the chemical potential is valid at zero temperature, we perform the experiment at a low temperature $T/T_F = 0.21(2)$. The value of γ at zero temperature [40] is initially input into Eq. (5) to calculate $b_x(t)$. Then we can obtain the cloud radius in the trap from the expansion data, $\langle x^2 \rangle_0 = \langle x(t)^2 \rangle_t / b(t)_x^2$, to determine the trapping potential energy U. We also measure the release energy E_{rel} from the long-time expansion. Using the energy relation, we obtain a new value of γ and input it into Eq. (5) for the next iterative calculation. We repeat the calculation until $|\gamma_{i+1} - \gamma_i|/\gamma_i \leq 10^{-5}$, where i denotes the number of iterations. The obtained γ in the BEC-BCS crossover is shown in Fig. 5(b). In the unitary regime, $\gamma \approx 2/3$. On the

BEC side, γ increases toward the molecule condensate limit with $\gamma = 1$. On the BCS side, γ decreases to some extent. The experimental measurements have the same variation trend with the mean field calculation at zero temperature [40]. The value of γ in the unitary regime does not change with temperature. But due to the finite-temperature effect, γ is smaller than the zero-temperature calculation on the BEC side, and on the BCS side it is larger. This can be reasonably understood that, as temperature increases, γ will change toward the thermal gas with $\gamma = 2/3$. γ could also be obtained by measuring the equation of state [43,44] and collective-mode oscillation [45].

With obtained γ, we can determine the cloud radius $\langle x^2 \rangle_0 = \gamma E_{\rm rel}/m\omega^2$. Three expansion behaviors in the BEC-BCS crossover are shown in Fig. 5(a), displaying the obvious deviation from that in the unitary regime $(1/k_{\rm F}a = 0)$ when the interaction strength is tuned away from the resonance. The expansion is fast on the BCS side $(1/k_{\rm F}a = -0.68)$ and slow on the BEC side $(1/k_{\rm F}a = 1.1)$, which can be well calculated with Eq. (6).

In conclusion, we observe the unique feature of the scale invariance induced by the coexistence of the spherical symmetry and unitary interaction, and demonstrate SO(2,1) symmetry of the system by observing the breathing mode. The virial theorem for the unitary Fermi gas has been verified. We also measure the effective exponent γ in the equation of state along the BEC-BCS crossover. The spherical unitary Fermi gas provides the platform to study geometrized quantum dynamics with SU(1,1) symmetry [46,47], nonequilibrium dynamics in the presence of conformal symmetry [48–50], and the bulk viscosity in the BEC-BCS crossover [51–53].

L. W., X. Y., and J. M. contributed equally to this work.

[*]Corresponding author: dlsun@wipm.ac.cn
[†]Corresponding author: kjjiang@wipm.ac.cn

[1] C. Chin, R. Grimm, P. Julienne, and E. Tiesinga, Feshbach resonances in ultracold gases, Rev. Mod. Phys. **82,** 1225 (2010).

[2] K. M. O'Hara, S. L. Hemmer, M. E. Gehm, S. R. Granade, and J. E. Thomas, Observation of a strongly interacting degenerate Fermi gas of atoms, Science **298,** 2179 (2002).

[3] J. Kinast, A. Turlapov, J. E. Thomas, Q. Chen, J. Stajic, and K. Levin, Heat capacity of a strongly interacting Fermi gas, Science **307,** 1296 (2005).

[4] S. Nascimbène, N. Navon, K. J. Jiang, F. Chevy, and C. Salomon, Exploring the thermodynamics of a universal Fermi gas, Nature (London) **463,** 1057 (2010).

[5] M. J. H. Ku, A. T. Sommer, L. W. Cheuk, and M. W. Zwierlein, Revealing the superfluid lambda transition in the universal thermodynamics of a unitary Fermi gas, Science **335,** 563 (2012).

[6] L. A. Sidorenkov, M. K. Tey, R. Grimm, Y.-H. Hou, L. Pitaevskii, and S. Stringari, Second sound and the superfluid fraction in a Fermi gas with resonant interactions, Nature (London) **498,** 78 (2013).

[7] A. B. Bardon, S. Beattie, C. Luciuk, W. Cairncross, D. Fine, N. S. Cheng, G. J. A. Edge, E. Taylor, S. Zhang, S. Trotzky, and J. H. Thywissen, Transverse demagnetization dynamics of a unitary Fermi gas, Science **344,** 722 (2014).

[8] B. Mukherjee, Z. Yan, P. B. Patel, Z. Hadzibabic, T. Yefsah, J. Struck, and M. W. Zwierlein, Homogeneous atomic Fermi gases, Phys. Rev. Lett. **118,** 123401 (2017).

[9] P. B. Patel, Z. Yan, B. Mukherjee, R. J. Fletcher, J. Struck, and M. W. Zwierlein, Universal sound diffusion in a strongly interacting Fermi gas, Science **370,** 1222 (2020).

[10] X. Li, X. Luo, S. Wang, K. Xie, X.-P. Liu, H. Hu, Y.-A. Chen, X.-C. Yao, and J.-W. Pan, Second sound attenuation near quantum criticality, Science **375,** 528 (2022).

[11] Z. Yan, P. B. Patel, B. Mukherjee, C. J. Vale, R. J. Fletcher, and M. W. Zwierlein, Thermography of the superfluid transition in a strongly interacting Fermi gas, Science **383,** 629 (2024).

[12] C. Menotti, P. Pedri, and S. Stringari, Expansion of an interacting Fermi gas, Phys. Rev. Lett. **89,** 250402 (2002).

[13] J. E. Thomas, J. Kinast, and A. Turlapov, Virial theorem and universality in a unitary Fermi gas, Phys. Rev. Lett. **95,** 120402 (2005).

[14] E. Elliott, J. A. Joseph, and J. E. Thomas, Observation of conformal symmetry breaking and scale invariance in expanding Fermi gases, Phys. Rev. Lett. **112,** 040405 (2014).

[15] S. Deng, Z.-Y. Shi, P. Diao, Q. Yu, H. Zhai, R. Qi, and H. Wu, Observation of the efimovian expansion in scale-invariant Fermi gases, Science **353,** 371 (2016).

[16] C. Cao, E. Elliott, H. Wu, and J. E. Thomas, Searching for perfect fluids: Quantum viscosity in a universal Fermi gas, New J. Phys. **13,** 075007 (2011).

[17] H. Guo, D. Wulin, C.-C. Chien, and K. Levin, Microscopic approach to shear viscosities of unitary Fermi gases above and below the superfluid transition, Phys. Rev. Lett. **107,** 020403 (2011).

[18] M. Bluhm, J. Hou, and T. Schäfer, Determination of the density and temperature dependence of the shear viscosity of a unitary Fermi gas based on hydrodynamic flow, Phys. Rev. Lett. **119,** 065302 (2017).

[19] C. Cao, E. Elliott, J. Joseph, H. Wu, J. Petricka, T. Schäfer, and J. E. Thomas, Universal quantum viscosity in a unitary Fermi gas, Science **331,** 58 (2011).

[20] E. Elliott, J. A. Joseph, and J. E. Thomas, Anomalous minimum in the shear viscosity of a Fermi gas, Phys. Rev. Lett. **113,** 020406 (2014).

[21] J. A. Joseph, E. Elliott, and J. E. Thomas, Shear viscosity of a unitary Fermi gas near the superfluid phase transition, Phys. Rev. Lett. **115,** 020401 (2015).

[22] F. Werner and Y. Castin, Unitary gas in an isotropic harmonic trap: Symmetry properties and applications, Phys. Rev. A **74**, 053604 (2006).

[23] See Supplemental Material at http://link.aps.org/supplemental/10.1103/PhysRevLett.132.243403 for the formation of an isotropic trap, measurement of the trapping frequency, determination of the atomic temperature and *in situ* atomic cloud size, fringe-removal analysis of the atomic images, hydrodynamic description of the atomic expansion from an isotropic trap, interaction effect on the ballistic expansion, and SO(2,1) symmetry, which includes Refs. [24–26].

[24] G. Veeravalli, E. Kuhnle, P. Dyke, and C. J. Vale, Bragg spectroscopy of a strongly interacting Fermi gas, Phys. Rev. Lett. **101**, 250403 (2008).

[25] L. Luo and J. E. Thomas, Thermodynamic measurements in a strongly interacting Fermi gas, J. Low Temp. Phys. **154**, 1 (2009).

[26] Y. Hou, L. P. Pitaevskii, and S. Stringari, Scaling solutions of the two-fluid hydrodynamic equations in a harmonically trapped gas at unitarity, Phys. Rev. A **87**, 033620 (2013).

[27] T.-L. Ho, Universal thermodynamics of degenerate quantum gases in the unitarity limit, Phys. Rev. Lett. **92**, 090402 (2004).

[28] D. T. Son, Vanishing bulk viscosities and conformal invariance of the unitary Fermi gas, Phys. Rev. Lett. **98**, 020604 (2007).

[29] M. A. Escobedo, M. Mannarelli, and C. Manuel, Bulk viscosities for cold Fermi superfluids close to the unitary limit, Phys. Rev. A **79**, 063623 (2009).

[30] K. Dusling and T. Schäfer, Bulk viscosity and conformal symmetry breaking in the dilute Fermi gas near unitarity, Phys. Rev. Lett. **111**, 120603 (2013).

[31] X. Yan, D. Sun, L. Wang, J. Min, S. Peng, and K. Jiang, Production of degenerate Fermi gases of ^{6}Li atoms in an optical dipole trap, Chin. Phys. Lett. **38**, 056701 (2021).

[32] X. Yan, D. Sun, L. Wang, J. Min, S. Peng, and K. Jiang, Observation of the BEC-BCS crossover in a degenerate Fermi gas of lithium atoms, Chin. Phys. B **31**, 016701 (2022).

[33] C. F. Ockeloen, A. F. Tauschinsky, R. J. C. Spreeuw, and S. Whitlock, Detection of small atom numbers through image processing, Phys. Rev. A **82**, 061606(R) (2010).

[34] F. Dalfovo, S. Giorgini, L. P. Pitaevskii, and S. Stringari, Theory of Bose-Einstein condensation in trapped gases, Rev. Mod. Phys. **71**, 463 (1999).

[35] M. J. Holland, D. S. Jin, M. L. Chiofalo, and J. Cooper, Emergence of interaction effects in Bose-Einstein condensation, Phys. Rev. Lett. **78**, 3801 (1997).

[36] R. Li, T. Gao, D. Zhang, S. Peng, L. Kong, X. Shen, and K. Jiang, Expansion dynamics of a spherical Bose–Einstein condensate, Chin. Phys. B **28**, 106701 (2019).

[37] L. P. Pitaevskii and A. Rosch, Breathing modes and hidden symmetry of trapped atoms in two dimensions, Phys. Rev. A **55**, R853 (1997).

[38] F. Chevy, V. Bretin, P. Rosenbusch, K. W. Madison, and J. Dalibard, Transverse breathing mode of an elongated Bose-Einstein condensate, Phys. Rev. Lett. **88**, 250402 (2002).

[39] E. Vogt, M. Feld, B. Fröhlich, D. Pertot, M. Koschorreck, and M. Köhl, Scale invariance and viscosity of a two-dimensional Fermi gas, Phys. Rev. Lett. **108**, 070404 (2012).

[40] H. Hu, A. Minguzzi, X.-J. Liu, and M. P. Tosi, Collective modes and ballistic expansion of a Fermi gas in the BCS-BEC crossover, Phys. Rev. Lett. **93**, 190403 (2004).

[41] S. Giorgini, L. P. Pitaevskii, and S. Stringari, Theory of ultracold atomic Fermi gases, Rev. Mod. Phys. **80**, 1215 (2008).

[42] H. Heiselberg, Collective modes of trapped gases at the BEC-BCS crossover, Phys. Rev. Lett. **93**, 040402 (2004).

[43] X. Wang, Y. Wu, X. Liu, Y. Wang, H. Chen, M. Maraj, Y. Deng, X.-C. Yao, Y.-A. Chen, and J.-W. Pan, Oscillatory-like expansion of a fermionic superfluid, Sci. Bull. **65**, 7 (2020).

[44] V. Navon and S. Nascimbène, F. Chevy, and C. Salomon, The equation of state of a low-temperature Fermi gas with tunable interactions, Science **328**, 5979 (2010).

[45] J. Kinast, A. Turlapov, and J. E. Thomas, Breakdown of hydrodynamics in the radial breathing mode of a strongly interacting Fermi gas, Phys. Rev. A **70**, 051401(R) (2004).

[46] C. Lyu, C. Lv, and Q. Zhou, Geometrizing quantum dynamics of a Bose-Einstein condensate, Phys. Rev. Lett. **125**, 253401 (2020).

[47] C. Lv, R. Zhang, and Q. Zhou, SU(1,1) echoes for breathers in quantum Gases, Phys. Rev. Lett. **125**, 253002 (2020).

[48] J. Maki and F. Zhou, Quantum many-body conformal dynamics: Symmetries, geometry, conformal tower states, and entropy production, Phys. Rev. A **100**, 023601 (2019).

[49] J. Maki and F. Zhou, Far-away-from-equilibrium quantum-critical conformal dynamics: Reversibility, thermalization, and hydrodynamics, Phys. Rev. A **102**, 063319 (2020).

[50] J. Maki, S. Zhang, and F. Zhou, Dynamics of strongly interacting Fermi gases with time-dependent interactions: Consequence of conformal symmetry, Phys. Rev. Lett. **128**, 040401 (2022).

[51] T. Enss, Bulk viscosity and contact correlations in attractive Fermi gases, Phys. Rev. Lett. **123**, 205301 (2019).

[52] J. Hofmann, High-temperature expansion of the viscosity in interacting quantum gases, Phys. Rev. A **101**, 013620 (2020).

[53] Y. Nishida, Viscosity spectral functions of resonating fermions in the quantum virial expansion, Ann. Phys. (Amsterdam) **410**, 167949 (2019).